Biochemical Engineering Journal 105 (2016) 71–79

Contents lists available at ScienceDirect

Biochemical Engineering Journal

journal homepage: www.elsevier.com/locate/bej

Regular article

Correlation among phenyltins molecular properties, degradation and cellular influences on *Bacillus thuringiensis* in the presence of biosurfactant

Litao Tang[a], Linlin Wang[a], Huase Ou[a], Qusheng Li[a], Jinshao Ye[a,*], Hua Yin[b,*]

[a] Key Laboratory of Environmental Exposure and Health of Guangzhou City, School of Environment, Jinan University, Guangzhou 510632, China
[b] College of Environment and Energy, South China University of Technology, Guangzhou 510006, China

ARTICLE INFO

Article history:
Received 27 April 2015
Received in revised form 5 September 2015
Accepted 15 September 2015
Available online 16 September 2015

Keywords:
Biodegradation
Biosorption
Biotransformation
Enzyme activity
Organotin
Ion

ABSTRACT

Although a successive dearylation is recognized as a triphenyltin biodegradation pathway, the cleavage pattern of the various chemical bonds of phenyltins is still not clear. Moreover, the correlation among phenyltins biosorption, degradation, molecular properties and metabolic impacts is far from fully understood. Therefore, phenyltins treatment of *Bacillus thuringiensis* was conducted. After degradation for 7 d in the presence of 50 mg L^{-1} of the surfactant sucrose fatty acid ester, the degradation efficiency of 1 mg L^{-1} triphenyltin reached its peak value of 89%. The surfactant altered the topological structure of the cellular peptide chains, accelerated triphenyltin binding and transport, increased cellular viability, Na^+/K^+- and Ca^{2+}/Mg^{2+}-ATPase activities, increased $PO_4^{3-}$and Na^+ assimilation, and decreased K^+ and Mg^{2+} release, resulting in the enhancement of triphenyltin degradation. However, surfactant did not change the successive dephenylation pathway, which was primarily determined by the bond energy of each Sn—C bond of triphenyltin

1. Introduction

Triphenyltin (TPT), an endocrine disruptor, is highly toxic to various invertebrates and vertebrates [1], and it is polluting the global environment as it is used worldwide. The high hydrophobicity and low solubility of TPT limit its access to microbes, resulting in its persistence in the ecosystem with a half-life varying from weeks to years [2]. Surfactants with hydrophobic and hydrophilic domains are capable of lowering TPT surface tension and enhancing its solubility, consequently leading to its high bioavailability. For example, some surfactants, such as sodium dihexylsulfosuccinate [3], rhamnolipid [4] and tea saponin [5], are found to obviously enhance organotin biodegradation. However, information regarding the influence of these surfactants on TPT molecular properties, biodegradation pathways, metabolite transformation, cell wall alteration and cellular metabolic responses is still very limited.

As an enzyme inhibitor and metabolic disproportionation compound [6], TPT may depress the metabolic activities involving its transport and degradation. Therefore, it is vital to investigate the regulation of cellular affinity, metabolism, and membrane permeability in the presence of surfactants during the TPT biodegradation process. As a biosurfactant with high biodegradability, surface-active properties and a wide use in the food, pharmaceutical and cosmetics industries [7], sucrose fatty acid ester (SFAE) was selected as a representative surfactant in the current study.

TPT biodegradation has been attributed to the joint processes of biosorption, transport and transformation. Among these steps, biosorption is an initial reaction and may be the limited step of TPT degradation because the structural and physicochemical relations between phenyltins (PTs) and the effective groups in the bacterial peptidoglycan layers play a key role in PTs binding, uptake and transformation [8]. Excessive alteration of the peptidoglycan structure induced by PTs could trigger significant apoptosis, whereas a lack of affinity between the cellular surface and PTs would limit PTs binding and transport. Thereby, it is necessary to investigate TPT binding to the cell surface.

To date, only a small number of bacterial strains have been identified as PTs-degrading microorganisms, such as *Bacillus thuringiensis* [5], *Brevibacillus brevis* [4] and *Stenotrophomonas maltophilia* [9]. However, the previous reports do not reveal why TPT transformation to monophenyltin (MPT) by these strains was faster than the further degradation of the produced MPT. The impact of different concentrations of surfactant on cellular metabolism,

* Corresponding authors.
E-mail addresses: jsye@jnu.edu.cn (J. Ye), huayin@scut.edu.cn (H. Yin).

http://dx.doi.org/10.1016/j.bej.2015.09.009
1369-703X/

cell wall structure, TPT transport, biosorption and transformation has seldom been illustrated. Therefore, the present work investigated TPT biosorption mechanisms and degradation pathways in the presence of SFAE and the correlation between degradation and molecular properties of pollutants. The viable biomass, ATPase activities, ion metabolism and cell morphology were analyzed to reveal cellular metabolic responses during the TPT degradation process by *B. thuringiensis*. The affinity between the cell wall peptidoglycan and TPT enhanced by SFAE was computed using ChemBio3D Ultra 13.0.

2. Materials and methods

2.1. Strain and chemicals

B. thuringiensis was isolated from organotin-bearing sediments collected at an e-waste processing town, Guiyu, in Guangdong Province, China. Triphenyltin chloride (purity = 98.8%) was purchased from Sigma–Aldrich (St. Louis, MO, USA). The concentrations of beef extract, peptone, NaCl and $MgSO_4$ in the culture medium were 3, 10, 5 and 0.03 g L^{-1}, respectively. The mineral salt medium (MSM) for TPT degradation contained (in mg L^{-1}) 150 $Na_2HPO_4{\cdot}12H_2O$, 50 KH_2PO_4, 30 NH_4Cl, 5 $Zn(NO_3)_2$ and 5 $MgSO_4$.

2.2. Microbial culture

B. thuringiensis was inoculated into 250 mL Erlenmeyer flasks with 100 mL culture medium at 30 °C on a rotary shaker at 130 rpm for 12 h. Subsequently, the cells were separated from the medium by centrifugation at 3500 × *g* for 10 min and were then washed three times with distilled water sterilized at 121 °C for 30 min.

2.3. TPT solubility enhancement by SFAE

The enhanced solubility of 1 mg L^{-1} TPT by SFAE at different concentrations up to 1000 mg L^{-1} was performed at 25 °C in 20 mL MSM by shaking on a rotary shaker at 100 rpm for 24 h. After equilibration for 12 h in the dark, the MSM was centrifuged at 3500 × *g* for 10 min. Subsequently, 10 mL of supernatant was transferred and extracted twice by hexane in an ultrasonic bath. The soluble TPT in the supernatant was detected according to Section 2.5.

2.4. TPT biodegradation, biosorption and adsorption

Twenty microliters of MSM containing 1 mg L^{-1} of TPT, the initial dosage of *B. thuringiensis* at 0.3 g L^{-1} and different concentration of SFAE (0–80 mg L^{-1}) were inoculated into a 250 mL Erlenmeyer flask in the dark at 25 °C on a rotary shaker at 100 rpm for 7 d. After degradation, the cells were separated and washed using phosphate buffer solution (PBS) for 20 min. TPT in PBS and inside of the cells represents TPT biosorption and accumulation, respectively. The total residual TPT in the MSM and cells was used to determine the degradation efficiency. To determine passive TPT binding by the cell surface, adsorption by dead cells inactivated by 2.5% glutaraldehyde for 24 h was evaluated under the same conditions. The controls were run in parallel in flasks that were not inoculated. All of the experiments were performed in triplicate, and the mean values were used in the calculations.

2.5. Analytical methods of PTs

After TPT degradation, PTs were analyzed by gas chromatography–mass spectrometry (QP2010, Shimadzu) equipped with a type Rxi-5MS GC column (30 m × 0.25 mm × 0.25 μm) [4]. Briefly, a constant flow rate of the carrier gas helium was set at 1.1 mL min^{-1}. The column temperature program started at 50 °C and held for 1.5 min. Subsequently, the oven was heated to 300 °C at a rate of 10 °C min^{-1} and held for 4 min. The solvent cut time was set to 2.6 min. The GC–MS interface temperature was maintained at 280 °C. Mass spectra were recorded at 1 scan s^{-1} under electronic impact with an electron energy of 70 eV and a mass range from 50 to 650 atoms to mass unit. The temperature of the ion source was set at 250 °C. Samples of 2 μL were injected directly.

2.6. Cellular morphology

The morphology of the cells before and after TPT degradation was observed by atomic force microscopy (AFM) and scanning electronic microscope (SEM) (Philips XL–30E). Briefly, the cells were deposited onto a glass surface and then air-fixed. Subsequently, the samples were mounted onto the XY stage of a commercial Autoprobe CP AFM, and the integral video camera was used to locate the observed regions. The imaging experiments were conducted in the tapping mode using a microfabricated silicon cantilever (Park Scientific Instruments).

Before SEM observation, the samples were fixed by glutaraldehyde for 24 h and sequentially dehydrated by ethanol at 20%, 50%, 70%, 90% and 100% (v/v). Then, the samples were immersed in isoamyl acetate for 30 min before dryness at the breakthrough point using CO_2 as a refrigerant. Subsequently, the samples were coated with gold to strengthen the conductivity and photographed by SEM.

2.7. Ion assimilation and release during TPT degradation

After degradation for 7 d, the cells were centrifuged at 3500 × *g* for 10 min. The resultant supernatant was filtered using a 0.22 μm polyether sulfone filter, and the concentrations of PO_4^{3-}, Na^+, K^+ and Mg^{2+} were detected using an ICS–900 ion chromatography system (Dionex, Sunnyvale, USA). The change in the ion concentration in MSM was calculated as the experimental content minus the control level; therefore, a negative value represents ion assimilation and a positive one represents ion release by the cells.

2.8. Analytical methods for ATPase activities

After TPT degradation, the cells were washed three times in cold PBS (pH 7.4), suspended in a cold lysis buffer (30 mM Tris–HCl, 7 M urea, 2 M thiourea, and 4% w/v 3-[(3-cholamidopropyl) dimethylammonio]-1-propane-sulfonate at pH 8.5) and lysed by sonication in an ice bath for 15 min. The cellular debris was removed from the suspension at 16,000 g for 5 min at 4 °C. Na^+/K^+- and Ca^{2+}/Mg^{2+}-ATPase activities were analyzed according to the instructions of the test kit, which was provided by the Nanjing Jiancheng Bioengineering Institute, China.

2.9. Cellular activities in carbon nutrient use after TPT degradation

Biolog microplates were used to analyze the cellular activities in carbon nutrient use after TPT degradation. The plates contained 96 wells with different carbon nutrients and a blank well without substrate. Each well had the redox dye tetrazolium, which could be reduced by the NADH generated by cellular metabolism. Briefly, 1 mL MSM was mixed with 99 mL of 0.85% sterilized saline solution. Next, 150 μL of the solution was inoculated into each well of the Biolog microplate and incubated at 25 °C in the dark. The optical density at 590 nm of each well was determined every 12 h. The Biolog data were calculated using an average well color development (AWCD) method.

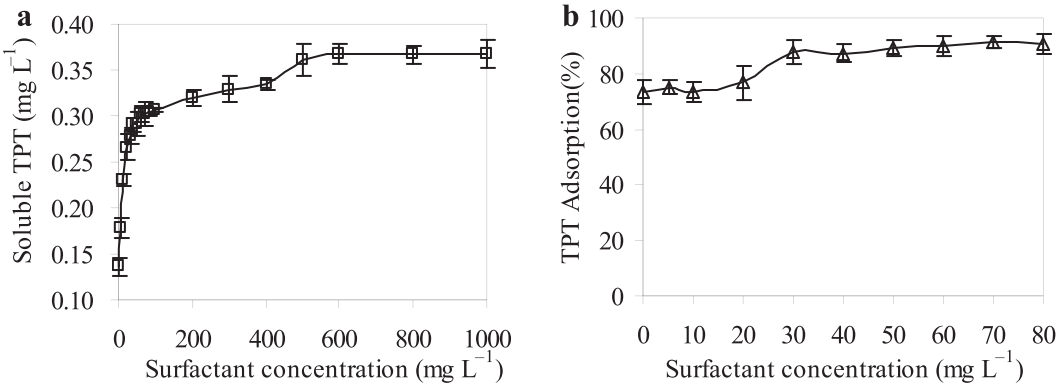

Fig. 1. Effect of SFAE on TPT solubility and adsorption (a) TPT solubility and (b) effect of SFAE on adsorption of 1 mg L^{-1} of TPT by inactivated *B. thuringiensis* cells for 7 d.

2.10. Computational methods

To further reveal TPT biosorption, the structures of TPT and the cell wall peptidoglycans were drawn using ChemBioDraw Ultra version 13.0 and then copied to ChemBio3D Ultra version 13.0 to create the three-dimensional model. Subsequently, these structures were subjected to energy minimization by molecular mechanics until the root-mean-square gradient became smaller than 0.01 kcal mol^{-1} Å. The interaction between TPT and the peptidoglycans was calculated by molecular dynamics. The step interval, frame interval and terminate of the calculation were 2 fs, 10 fs and 10,000 steps, respectively.

2.11. Statistical analysis

The mean values of triplicate samples were used in the calculations of TPT biodegradation, biosorption and adsorption, and cellular metabolic activities using SPSS 13.0 software. The statistical analysis of the correlation between TPT treatment and metabolic activities was performed by SPSS using Pearson correlation tests.

3. Results

3.1. Effect of SFAE on TPT solubility and adsorption

SFAE in the range of 5–1000 mg L^{-1} strongly emulsified TPT with both lipophilic and polar moieties, ascending the dissolved TPT from 0.14 to 0.37 mg L^{-1} (Fig. 1a). To determine whether the increase in dissolved TPT enhances the contact between TPT and the cells, TPT adsorption by dead cells was determined (Fig. 1b). However, the analysis of variance revealed that when the SFAE concentration was lower than 20 mg L^{-1}, the adsorption efficiency was not significantly different than the control (Table S1). These results verify that the influence of the enhanced TPT solubility in the presence of SFAE at 5–20 mg L^{-1} on TPT adsorption can be ignored. The increasing concentration of soluble TPT with increasing surfactant encouraged the interaction of TPT with the cellular surface, resulting in higher TPT adsorption (Fig. 1b).

3.2. TPT degradation, surface binding and accumulation

TPT degradation exhibited an ascending trend from 63% to 89% when the concentration of SFAE was increased from 5 to 50 mg L^{-1} (Fig. 2a). Meanwhile, TPT biosorption by the cell surface showed a descending trend. Next, this biosorption increased in the presence of SFAE at 60–80 mg L^{-1}. Although further increasing the SFAE concentration depressed TPT degradation compared to the low level of SFAE, it still enhanced the degradation in comparison with the control. However, 35–164 μg L^{-1} of TPT was accumulated with the reverse trend of TPT degradation. Fig. 2b shows that the biomass of the viable cells at 7 d was rising with SFAE concentration. The pH value was maintained from 6.44 to 6.67 and was not significantly affect by SFAE ($p = 0.849$). According to the results of the TPT degradation, metabolite concentration and viable cells, the optimum concentration for SFAE to enhance TPT transformation is 50 mg L^{-1}.

The backbone of the peptidoglycan strands is a repeating unit of *N*-acetylglucosamine linked to *N*-acetylmuramic acid through a β-1,4-glycosidic bond. In each *N*-acetylmuramic acid there is a pentapeptide attached to the D-lactyl moiety. This peptide chain is connected with another peptidoglycan chain creating a crosslink which forms the cell wall polymer. The attachments of the side chain –N(H)–C(O)–CH_3 and wall teichoic acids exhibited intense affinity for TPT (Fig. 2c). SFAE altered the topological structure of the peptidoglycans through the interaction between its hydrophobic domain and the peptides of the peptidoglycans and also through the affinity between the hydrophilic domain and *N*-acetylglucosamine (Fig. 2d).

3.3. Cellular morphology

Fig. 3a shows that the cells displayed a plump shape with an intact and smooth cell wall, which is beneficial for maintaining cellular metabolic activities and TPT degradation abilities [4,10]. The morphology of the cells exposed to 50 mg L^{-1} of SFAE (Fig. 3b) did not show obvious differences from the control, whereas the cells post-TPT degradation were surrounded by many granules (Fig. 3c).

The cellular morphology observed using SEM confirmed that the cells cultured in solution with 50 mg L^{-1} of SFAE displayed the same morphology as the control sample (Fig. 3d and e). However, TPT exposure did have a detrimental effect on *B. thuringiensis* and induced the death of certain cells, releasing their endospores into the MSM (Fig. 3f). Compared with the control cells (Fig. 3d), the morphology of the viable cells in MSM for 7 d (Fig. 3f) was significantly different, showing cell wall wrinkles.

3.4. Ion and organic carbon metabolism by cells during TPT degradation

Without SFAE in MSM, all of the detected ions were released by the cells (Fig. 4a). SFAE shifted PO_4^{3-} and Na^+ from release to assimilation and decreased Mg^{2+} efflux. The K^+ concentration tended to increase with the increase of the SFAE level, but was still lower than without SFAE.

The Biolog plates contain 31 species of carbon substrates that were classified into 6 classes as carbohydrates, esters, alcohols, carboxylic acids, amino acids and amines to investigate the effect of SFAE on carbon usage. Fig. 4b displays an obviously elevated trend of organic carbon assimilation in the presence of SFAE. Fig.

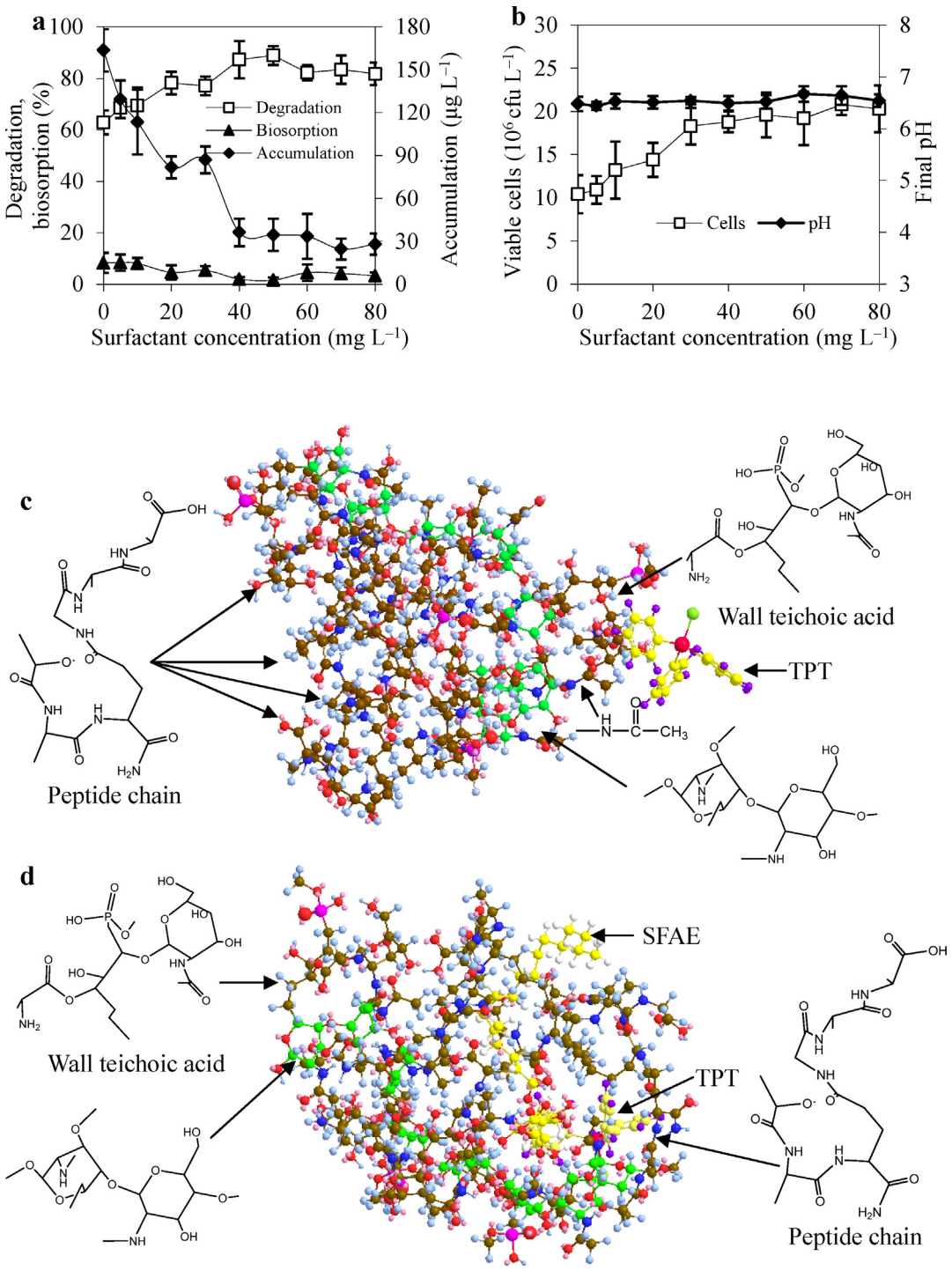

Fig. 2. TPT degradation, surface binding and accumulation by *B. thuringiensis* with 5–80 mg L^{-1} of SFAE for 7 d (a) TPT degradation, surface binding and accumulation, (b) final pH value and cell viability after TPT degradation, (c) TPT binding by effective moieties of the cell wall and (d) TPT transport across the cell wall accelerated by SFAE.

S1 reflects that the metabolic activities of *B. thuringiensis* on the use of all of the classes of carbons were obviously increased in the presence of SFAE.

3.5. ATPase activities during TPT biodegradation

Na^+/K^+- and Ca^{2+}/Mg^{2+}-ATPase activities had similar increasing tendencies in the presence of SFAE at 5–50 mg L^{-1} (Fig. 5). Subsequently, the activities declined when the level of SFAE increased to 60–80 mg L^{-1}, but the activities still increased in comparison with the control. The Pearson correlation analysis demonstrated that Na^+/K^+- and Ca^{2+}/Mg^{2+}-ATPase activities are significantly correlated with TPT degradation.

3.6. TPT metabolites and their further biodegradation

Fig. 6a reveals that TPT was transformed into the less toxic metabolites DPT and MPT. The residual concentration of these PTs after degradation is in the following order: TPT > DPT > MPT (Fig. 6a and b). To further reveal the dearylation pathway, TPT degradation

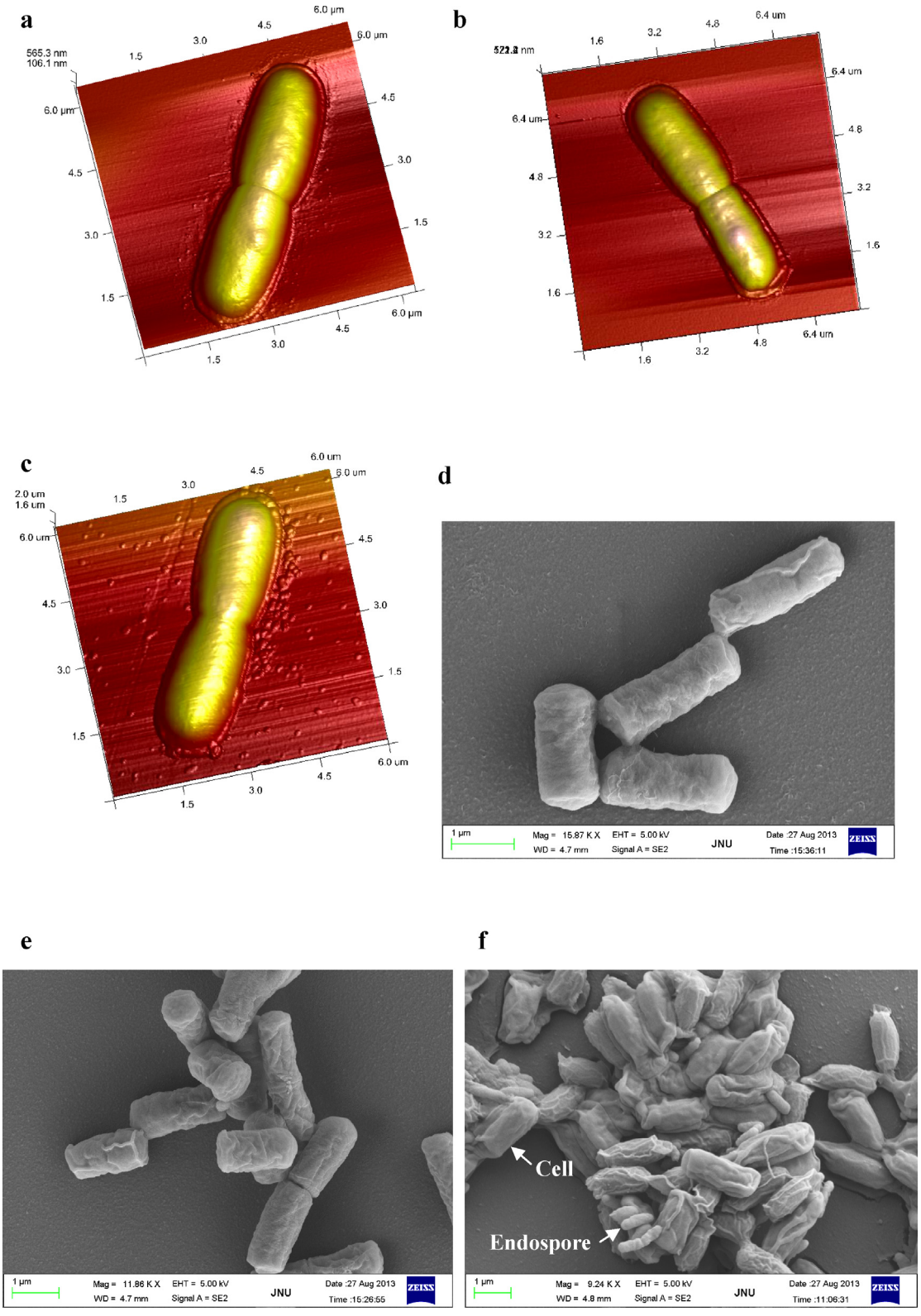

Fig. 3. Surface morphology of *B. thuringiensis* (a) control cells observed using AFM, (b) cells cultured in solution with 50 mg L^{-1} of SFAE observed using AFM, (c) *B. thuringiensis* observed using AFM after TPT degradation in the presence of 50 mg L^{-1} of SFAE, (d) control cells observed using SEM, (e) cells cultured in solution with 50 mg L^{-1} of SFAE observed using SEM and (f) *B. thuringiensis* and endospores observed using SEM after TPT degradation in the presence of 50 mg L^{-1} of SFAE.

by *B. thuringiensis* in the presence of 50 mg L^{-1} of SFAE at 1–7 d was performed (Fig. 6c). The amount of MPT produced on the first day was less than 40 μg L^{-1} and accumulated on the third day. As for the generated DPT, its concentration was higher than MPT and almost linearly declined during the process, which illustrates that TPT dearylation occurred successively.

This dearylation pattern primarily resulted from the fact that the topological structure of PTs is asymmetric and the energy of

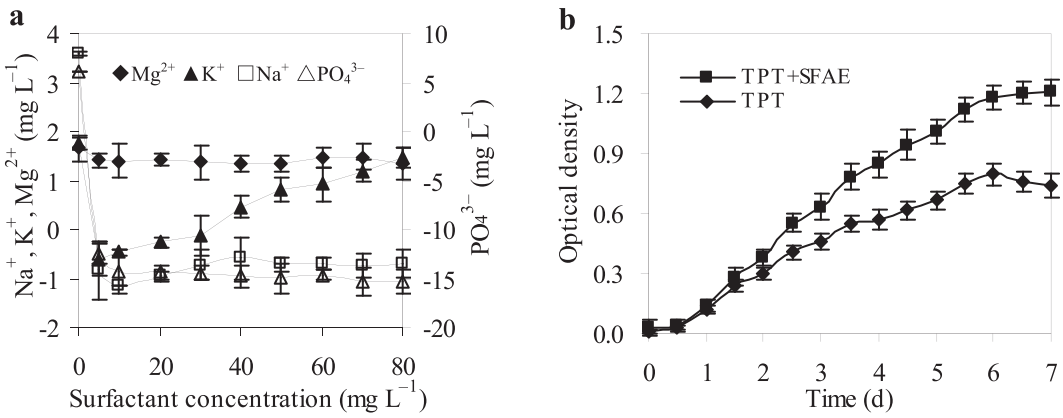

Fig. 4. Effect of SFAE on ion metabolism and organic carbon use by *B. thuringiensis* after TPT degradation for 7 d (a) ion assimilation and release and (b) activities of organic carbon use by cells.

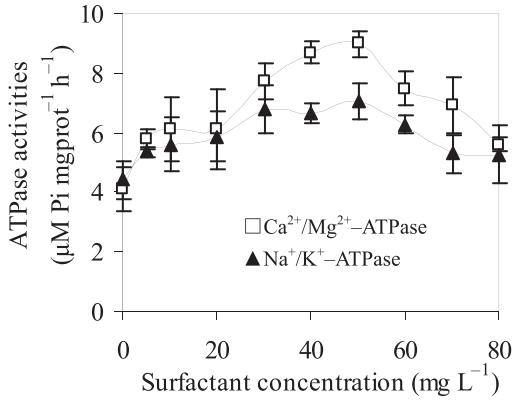

Fig. 5. Na^+/K^+- and Ca^{2+}/Mg^{2+}-ATPase activities of *B. thuringiensis* after TPT degradation for 7 d.

each Sn—C bond is different (Table S2–4). Among all of the covalent bonds linking Sn and C in PTs, the one in MPT contained the highest bond energy, whereas the total energy of MPT is lower than that of DPT and TPT (Table S5). When compared with HOMO of benzene, more pairs of electrons were shared between tin and its linked carbon (Fig. 6d), reducing the number of electrons shared among C(3), C(4) and C(5) in the benzene rings of PTs. The HOMO–LUMO energy gap of benzene is wider than that of PTs (Table S5).

4. Discussion

TPT binding by the dead cells was independent of metabolism, primarily relying on TPT solubility, membrane permeability and the interaction of hydrophobic TPT with membrane constituents (Fig. 1b), which has been demonstrated by the biodegradation of other trisubstituted organotins. For example, tributyltin (TBT) could induce a significant change in the fatty acid composition of *Cunninghamella elegans* [11]. TBT and its metabolites were inferred to be bound to the cell membrane lipids of *Aeromonas veronii* during the TBT degradation process [12]. The computational results infer that TPT tends to be attracted by the C-terminal tail of $–N(H)–C(O)–CH_3$ and the hydrocarbon chain of the wall teichoic acid due to their lipophilic properties (Fig. 2c). The structure of the peptidoglycan mimic has a helical periodicity of 30 Å and a 70 Å diameter pore in the middle of each hexagonal unit [8], which implies that TPT can transport across the cell wall easily after surface binding because the diameter of TPT is less than 11 Å. The alteration triggered by SFAE formed 15 Å diameter pores among the peptidoglycans, accelerating TPT transport (Fig. 2d).

Due in part to the increase in TPT solubility and adsorption induced by SFAE, the dissolved TPT uptake into the cytoplasm through diffusion and active transport may be enhanced, which encourages TPT degradation because it takes place intracellularly [4,13]. Furthermore, the regulation of cellular hydrophobicity by SFAE improves the affinity of *B. thuringiensis* to TPT, which further accelerates the transportation of dissolved TPT.

As a biodegradable surfactant stemming from an acylation or esterification reaction between sucrose and fatty acids, SFAE serves as a nutrient for cellular metabolism and is also partially responsible for the improvement of TPT degradation. This hypothesis has been confirmed by the correlation between surfactant assimilation and TPT degradation [4]. Although the supplemental organic nutrients at low concentrations increased organotin biodegradation, the excessive assimilation of these substrates at high levels could trigger a decreasing degradation of the target contaminant [4,14], which is also consistent with the function of SFAE as a nutrient at different concentrations in the current experiment (Fig. 2b).

The above-mentioned influence of nutrients at different concentrations might be attributed to the change in pH induced by nutrient assimilation [15,16] because a low pH has a detrimental effect on TPT biosorption by *B. brevis* [4] and the persistence of TPT appears to be pH-dependent [17]. However, the stable pH value after TPT degradation suggests that the decreasing efficiency of TPT degradation in the presence of SFAE at 60–80 mg L^{-1} is not attributed to the pH change but to the excessive use of SFAE (Fig. 2b).

Although SFAE at 60–80 mg L^{-1} inhibited the further enhancement of TPT degradation (Fig. 2a), the decline in TPT accumulation illustrates that high levels of SFAE helped to regulate cellular metabolism under TPT exposure by converting intracellular TPT to MSM or by depressing the transport of extracellular TPT. A portion of metabolites transported from the interior to the cellular surface during TBT degradation is also consistent with our findings [18]. The increase in TPT binding in the presence of SFAE at 60–80 mg L^{-1}, as shown in Fig. 2a, also confirms that high levels of SFAE inhibited TPT transport to some extent.

Although any change in the surrounding conditions will influence microbial responses, the morphology of viable cells after TPT degradation did not display apparent differences compared with the control cells (Fig. 3a–c). However, TPT did enhance the permeability of the cell surface, improve the excretion of intracellular substances, and even trigger the apoptosis of some cells (Fig. 3f). A previous investigation of TPT degradation by *B. brevis* also found cellular apoptosis after PTs exposure [4]. However, the AFM observation showed that the cells under TPT stress did not have the same wrinkled appearance as those under SEM observation. The unique abilities of working in a near-physiological environment combined

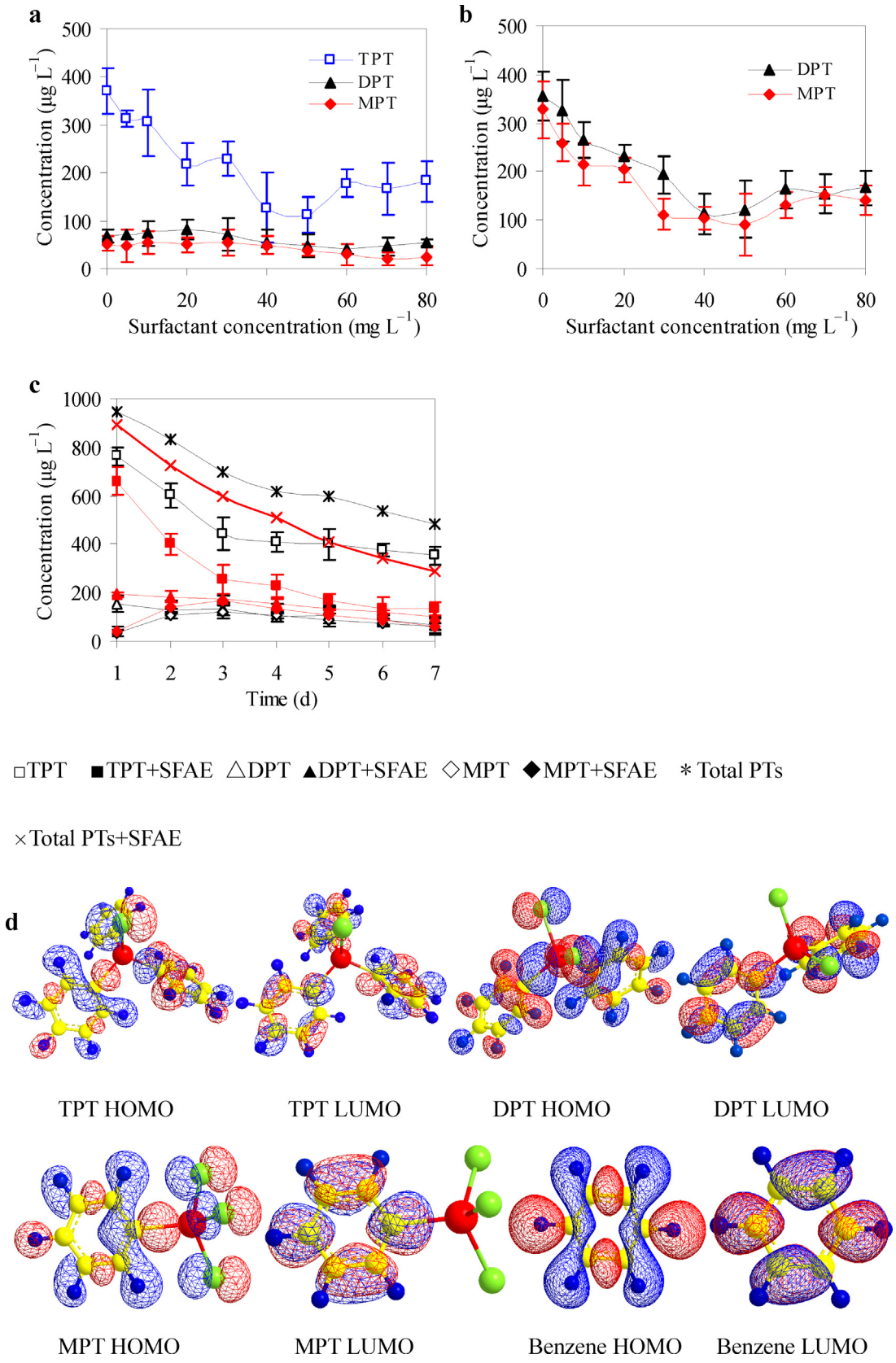

Fig. 6. Degradation of PTs at 1 mg L^{-1} by *B. thuringiensis* with SFAE at 0–80 mg L^{-1} (a) PTs concentration after TPT degradation for 7 d, (b) DPT and MPT degradation for 7 d, (c) TPT degradation by *B. thuringiensis* with or without 50 mg L^{-1} of SFAE for 1–7 d and (d) highest occupied molecular orbital (HOMO) and lowest occupied molecular orbital (LUMO) of PTs and benzene.

with excellent resolution make AFM a powerful method to observe cellular morphology [19], whereas samples for SEM observation need to be dehydrated and dried. Therefore, the difference in morphology between Fig. 3c and f illustrates that the exposure to TPT did not induce the detectable change in the cellular surface of the viable cells but did trigger the release of intracellular materials (Fig. 4) or the degradation of macromolecules, which may be related to the cellular wrinkles after dehydration for SEM observation.

Concerning the release of intracellular materials, some published studies have found that TPT can accumulate in the lipid and erythrocyte membrane [20,21], causing an efflux of some cytosolic ions [22]. Mg^{2+} release is likely due to cellular apoptosis (Fig. 3f) or the degradation of some Mg^{2+}-binding molecules after TPT exposure [24]. SFAE increased the viable cells consuming Mg^{2+} and reduced the efflux of Mg^{2+} accordingly (Fig. 4a). The biomass increase and TPT degradation enhancement by SFAE (Fig. 2) accordingly accelerated high-energy phosphate conversion, triggering PO_4^{3-} transport. The uptake accumulated PO_4^{3-} against its thermodynamic gradient by cotransport with Na^+[23], which is consistent with Na^+ assimilation in the current study (Fig. 4a). The Na^+/K^+-ATPase is the mediator that transports Na^+ and K^+ in the opposite direction [22]. K^+ shifts from assimilation to release with the SFAE increase from 5 to 80 mg L^{-1}, while Na^+ always has an assimilation trend related to Na^+ and K^+ transport by the Na^+/K^+-ATPase.

Na^+/K^+- and Ca^{2+}/Mg^{2+}-ATPases are two ATP-hydrolyzing enzymes which maintain ion gradients that are essential for signal transduction and active transport [25]. Their activities are altered by exposure to xenobiotics through the disruption of energy-producing pathways or the direct interaction with the enzymes [26,27]. For example, Na^+/K^+-ATPase activity in the gill and brain of *Cirrhinus mrigala* under mercuric chloride stress was found to be significantly decreased [27]. Exposure to 2-chloroethylethyl sulfide also led to a dose-dependent decrease in Ca^{2+}/Mg^{2+}-ATPase activity by alkylating the enzyme [28]. Therefore, the ATPase activity may be used as an index to determine tolerable levels of contaminants [27]. A similar inhibition of ATPase activities was also exhibited in the current study without SFAE (Fig. 5). The significant correlation between TPT degradation and the activities of Na^+/K^+- and Ca^{2+}/Mg^{2+}-ATPases ($p = 6.9 \times 10^{-16}$, 1.0×10^{-15}) in the presence of SFAE confirmed that ATPase activity is a key indicator of TPT degradation.

The Na^+/K^+-ATPase returns Na^+ and K^+ concentrations to a primary transmembrane level in the developing electrochemical gradient, which is essential for active transport and intracellular pH regulation [29]. Therefore, the activation of these ATPases by SFAE accelerated TPT transport and degradation (Fig. 2a) and increased ion influx (Fig. 4). The phosphorylation and dephosphorylation undergone by the Na^+/K^+- and Ca^{2+}/Mg^{2+}-ATPases during the enhanced TPT degradation process were accelerated by SFAE, triggering the increase in PO_4^{3-} transport, which is consistent with PO_4^{3-} assimilation in the presence of SFAE (Fig. 4).

Thus far, although a successive dearylation is recognized as a pathway of TPT biodegradation [30], whether dephenylation synchronously occurs is still not clear. The observations from environmental monitoring and TPT degradation suggest that MPT has often been the predominant species of PTs in the samples, whereas DPT was rarely found [17,31,32]. TPT transformation by *B. brevis* and dibutyltin degradation by *Streptomyces* sp. also showed similar results [4,33]. Therefore, TPT → DPT → MPT transformation is considered to be the quick process with regard to MPT → tin [17]. However, the concentration of MPT is lower than that of DPT in the current experiment (Fig. 6a). It seems that the cleavage reactions sequentially occur in the benzene rings of TPT. As for the complexity of the molecular structure of PTs, MPT is the simplest one, so it is easily utilized by bacteria. Due to the DPT accumulation, it can be deduced that MPT dephenylation is not the efficiency-controlling step in TPT degradation (Fig. 6b). The trend of the DPT concentration illustrates that the generated DPT was further degraded (Fig. 6c). However, the initial level of MPT is very low, which is related to the fast transformation of MPT to tin or the slow production of MPT during TPT and DPT degradation on the first day (Fig. 6c).

The molecular properties of PTs and benzene computed by ChemBio Office reveal that the bond between the anionic species and tin was the easiest to hydrolyze due to containing the lowest bond energy. The cleavage occurred in the Sn—C bonds of TPT and DPT individually, not synchronously. Due to the low total energy of MPT, the produced MPT is less than DPT (Fig. 6c). The SFAE accelerated TPT transformation and increased metabolite production, but it did not change the dephenylation pathway. The degradation of the tin-linked rings initially occurred in the cleavage of the C(3)–C(4) or C(4)–C(5) band. The energy needed for a ground state electron of benzene to jump to the excited state is obviously higher than that of PTs, which means that the cleavage of the benzene ring in PTs can occur more easily than benzene degradation.

5. Conclusions

The cleavage occurred in the Sn—C bonds of TPT and DPT individually, and the degradation of these tin-linked benzenes initially occurred in the cleavage of the C(3)–C(4) or C(4)–C(5) band. The SFAE altered the topological structure of the peptide chains of the cell wall, enhanced TPT solubility, adsorption, transport and degradation, increased cell viability and ATPase activities, reduced K^+ and Mg^{2+} release, and shifted $PO_4^{3-}$and Na^+ from release to assimilation, but it did not change the dephenylation pathway. According to the TPT degradation, metabolite concentration, cell viability and ATPase activities, the optimum concentration for SFAE to enhance TPT transformation is 50 mg L^{-1}. After degradation for 7 d by *B. thuringiensis* and 50 mg L^{-1} of SFAE, the degradation efficiency of 1 mg L^{-1} TPT reached its peak value of 89%. These findings present new insights into the correlation among phenyltins biosorption, degradation, metabolic impacts, cell wall structure and pollutant molecular properties.

Acknowledgements

The authors would like to thank the National Natural Science Foundation of China (Nos. 21377047, 21577049), the Science and Technology Project of Guangdong Province (Nos. 2014A020216013, 2014A020216014), and the Fundamental Research Funds for the Central Universities (No. 21615459) for their financial support.

Appendix A. Supplementary data

Supplementary data associated with this article can be found, in the online version, at http://dx.doi.org/10.1016/j.bej.2015.09.009.

References

[1] F.G. Antes, E. Krupp, E.M.M. Flores, V.L. Dressler, J. Feldmann, Speciation and degradation of triphenyltin in typical paddy fields and its uptake into rice plants, Environ. Sci. Technol. 45 (2011) 10524–10530.
[2] L.Ó. GuÞmundsdóttir, K.K.Y. Ho, J.C.W. Lam, J. Svavarsson, K.M.Y. Leung, Long-term temporal trends (1992–2008) of imposex status associated with organotin contamination in the dogwhelk *Nucella lapillus* along the Icelandic coast, Mar. Pollut. Bull. 63 (2011) 500–507.
[3] L. Mathurasa, C. Tongcumpou, D.A. Sabatini, E. Luepromchai, Anionic surfactant enhanced bacterial degradation of tributyltin in soil, Int. Biodeter. Biodegr. 75 (2012) 7–14.
[4] J.S. Ye, H. Yin, H. Peng, J.Q. Bai, D.P. Xie, L.L. Wang, Biosorption and biodegradation of triphenyltin by *Brevibacillus brevis*, Bioresource Technol. 129 (2013) 236–241.
[5] J. Huang, J.S. Ye, J.W. Ma, J. Gao, S.Q. Chen, X.L. Wu, Triphenyltin biosorption, dephenylation pathway and cellular responses during triphenyltin

biodegradation by *Bacillus thuringiensis* and tea saponin, Chem. Eng. J. 249 (2014) 167–173.
[6] M. Fickova, L. Macho, J. Brtko, A comparison of the effects of tributyltin chloride and triphenyltin chloride on cell proliferation, proapoptotic p53, Bax, and antiapoptotic Bcl-2 protein levels in human breast cancer MCF-7 cell line, Toxicol. In Vitro 29 (2015) 727–731.
[7] Y.C. Meng, M.H. Sun, S. Fang, J. Chen, Y.H. Li, Effect of sucrose fatty acid esters on pasting, rheological properties and freeze–thaw stability of rice flour, Food Hydrocolloid. 40 (2014) 64–70.
[8] S.J. Kim, J. Chang, M. Singh, Peptidoglycan architecture of gram-positive bacteria by solid-state NMR, BBA–Biomembranes 1848 (2015) 350–362.
[9] J. Gao, J.S. Ye, J.W. Ma, L.T. Tang, J. Huang, Biosorption and biodegradation of triphenyltin by *Stenotrophomonas maltophilia* and their influence on cellular metabolism, J. Hazard. Mater. 276 (2014) 112–119.
[10] J.S. Ye, H. Yin, B.X. Mai, H. Peng, H.M. Qin, B.Y. He, N. Zhang, Biosorption of chromium from aqueous solution and electroplating wastewater using mixture of *Candida lipolytica* and dewatered sewage sludge, Bioresource Technol. 101 (2010) 3893–3902.
[11] P. Bernat, J. Długoński, Tributyltin chloride interactions with fatty acids composition and degradation ability of the filamentous fungus *Cunninghamella elegans*, Int. Biodeter. Biodegr. 60 (2007) 133–136.
[12] A. Cruz, T. Caetano, S. Suzuki, S. Mendo, *Aeromonas veronii*, a tributyltin (TBT)—degrading bacterium isolated from an estuarine environment Ria de Aveiro in Portugal, Mar. Environ. Res. 64 (2007) 639–650.
[13] A. Ortiz, J.A. Teruel, F.J. Aranda, Effect of triorganotin compounds on membrane permeability, BBA–Biomembranes 1720 (2005) 137–142.
[14] A.S. Stasinakis, N.S. Thomaidis, A. Nikolaou, A. Kantifes, Aerobic biodegradation of organotin compounds in activated sludge batch reactors, Environ. Pollut. 134 (2005) 431–438.
[15] R.W. Hunziker, B.I. Escher, R.P. Schwarzenbach, pH dependence of the partitioning of triphenyltin and tributyltin between phosphatidylcholine liposomes and water, Environ. Sci. Technol. 35 (2001) 3899–3904.
[16] A. Sakultantimetha, H.E. Keenan, T.K. Beattie, T.J. Aspray, S. Bangkedphol, A. Songsasen, Acceleration of tributyltin biodegradation by sediment microorganisms under optimized environmental conditions, Int. Biodeter. Biodegr. 64 (2010) 467–473.
[17] C. Marcic, I.L. Hecho, L. Denaix, G. Lespes, TBT and TPhT persistence in a sludged soil, Chemosphere 65 (2006) 2322–2332.
[18] N.F.Y. Tam, A.M.Y. Chong, Y.S. Wong, Removal of tributyltin (TBT) by live and dead microalgal cells, Mar. Pollut. Bull. 45 (2002) 362–371.
[19] C.Z. Wang, V.K. Yadavalli, Investigating biomolecular recognition at the cell surface using atomic force microscopy, Micron 60 (2014) 5–17.
[20] D. Bonarska-Kujawa, H. Kleszczyńska, S. Przestalski, The location of organotins within the erythrocyte membrane in relation to their toxicity, Ecotox. Environ. Saf. 78 (2012) 232–238.
[21] D. Man, Fluidity of liposome membranes doped with organic tin compounds: ESR study, J. Liposome Res. 18 (2008) 225–234.
[22] J.L.E. Monti, M.R. Montes, R.C. Rossi, Alternative cycling modes of the Na^+/K^+-ATPase in the presence of either Na^+ or Rb^+, BBA–Biomembranes 1828 (2013) 1374–1383.
[23] R. Zvyagilskaya, B.L. Persson, A novel alkali—tolerant *Yarrowia lipolytica* strain for dissecting Na^+-coupled phosphate transport systems in yeasts, Cell Biol Int. 29 (2005) 87–94.
[24] A. Romani, Regulation of magnesium homeostasis and transport in mammalian cells, Arch. Biochem. Biophys. 458 (2007) 90–102.
[25] L. Ji, A. Chauhan, W.T. Brown, V. Chauhan, Increased activities of Na^+/K^+-ATPase and Ca^{2+}/Mg^{2+}-ATPase in the frontal cortex and cerebellum of autistic individuals, Life Sci. 85 (2009) 788–793.
[26] B. Burlando, M. Bonomo, F. Caprì, G. Mancinelli, G. Pons, A. Viarengo, Different effects of Hg^{2+} and Cu^{2+} on mussel (*Mytilus galloprovincialis*) plasma membrane Ca^{2+}-ATPase: Hg^{2+} induction of protein expression, Comp. Biochem. Phys. C 139 (2004) 201–207.
[27] R.K. Poopal, M. Ramesh, B. Dinesh, Short-term mercury exposure on Na^+/K^+-ATPase activity and ionoregulation in gill and brain of an Indian major carp, *Cirrhinus mrigala*, J. Trace Elem. Med. Bio. 27 (2013) 70–75.
[28] Y.B. Kim, Y.S. Lee, D.S. Choi, S.H. Cha, D.E. Sok, Inactivation of microsomal Ca^{2+}-ATPase by 2-chloroethylethyl sulfide, Chem. Biol. Interact. 97 (1995) 239–246.
[29] M. Havlíková, M. Huličiak, V. Bazgier, K. Berka, M. Kubala, Fluorone dyes have binding sites on both cytoplasmic and extracellular domains of Na, K-ATPase, BBA–Biomembranes 1828 (2013) 568–576.
[30] G.I. Paton, W. Cheewasedtham, I.L. Marr, J.J.C. Dawson, Degradation and toxicity of phenyltin compounds in soil, Environ. Pollut. 144 (2006) 746–751.
[31] C. Bancon-Montigny, G. Lespes, M. Potin-Gautier, Organotin survey in the Adour–Garonne basin, Water Res. 38 (2004) 933–946.
[32] J. Heroult, Y. Nia, L. Denaix, M. Bueno, G. Lespes, Kinetic degradation processes of butyl—and phenyltins in soils, Chemosphere 72 (2008) 940–946.
[33] P. Bernat, J. Długoński, Isolation of *Streptomyces* sp. strain capable of butyltin compounds degradation with high efficiency, J. Hazard. Mater. 171 (2009) 660–664.